

Proceedings Article

Rapid TAURUS for Real-Time Color MPI: A Feasibility Study

Musa Tunç Arslan ^{a,b,*}, Emine Ulku Saritas ^{a,b,c}

^aDepartment of Electrical and Electronics Engineering, Bilkent University, Ankara, Turkey

^bThe National Magnetic Resonance Research Center (UMRAM), Bilkent University, Ankara, Turkey

^cSabuncu Brain Research Center, Bilkent University, Ankara, Turkey

*Corresponding author, email: mtarslan@ee.bilkent.edu.tr

© 2022 Arslan *et al.*; licensee Infinite Science Publishing GmbH

This is an Open Access article distributed under the terms of the Creative Commons Attribution License (<http://creativecommons.org/licenses/by/4.0>), which permits unrestricted use, distribution, and reproduction in any medium, provided the original work is properly cited.

Abstract

Recent developments in color magnetic particle imaging (MPI) provided additional functionalities to MPI, such as distinguishing magnetic nanoparticles (MNPs) by type or by their environmental conditions. In this work, we propose rapid TAURUS (TAU estimation via Recovery of Underlying mirror Symmetry) to achieve relaxation-based real-time color MPI. The method can successfully map the effective relaxation time constants in a relatively wide field-of-view (FOV) at frame rates exceeding 5 frames-per-second (FPS). We present the first simulation results demonstrating that rapid TAURUS is capable of generating high fidelity and high FPS color MPI images in real time.

I. Introduction

Color Magnetic Particle Imaging (MPI) offers a means to distinguish different magnetic nanoparticles (MNPs) with potential applications such as catheter tracking [1], temperature mapping [2], and viscosity mapping [3, 4]. Real-time color MPI can provide a safe alternative to x-ray fluoroscopy for catheter tracking during cardiovascular interventions [1], and a fast alternative to magnetic resonance imaging for the diagnosis of stroke [5].

We previously proposed TAURUS (TAU estimation via Recovery of Underlying mirror Symmetry) for relaxation-based color MPI [4, 6], and boosted its performance to make it applicable for rapid and multi-dimensional trajectories [7]. Rapid TAURUS utilizes time-varying focus fields (FFs) to rapidly scan a field-of-view (FOV), and corrects the FF-induced distortions on the signal before estimating the effective relaxation time constant, τ [7].

In this work, we present the first simulation results for real-time color MPI using rapid TAURUS. For a 5×6 cm² field-of-view (FOV), we demonstrate frame rates exceeding 5 frames-per-second (FPS). We also show that higher

frames can be achieved by zooming into a smaller region of interest (ROI). The results demonstrate the feasibility of real-time color MPI using rapid TAURUS.

II. Methods and Materials

II.1. Rapid TAURUS

Figure 1 shows an example 2D triangle trajectory used in this work, with a triangle shaped FF along the x-direction and a linearly ramping FF along the z-direction:

$$\mathbf{x}_s(t) = \begin{bmatrix} \frac{\text{FOV}_x}{\pi} \sin^{-1}(\sin(2\pi f_T t)) \\ 0 \\ \frac{R_{s,z} t}{G_z} \end{bmatrix} + \begin{bmatrix} 0 \\ 0 \\ \frac{B_p}{G_z} \cos(2\pi f_d t) \end{bmatrix}. \quad (1)$$

Here, $\mathbf{x}_s(t)$ is the field free point (FFP) position, $f_T = R_{s,x}/(2\text{FOV}_x G_x)$ is the frequency of the triangle wave, and B_p and f_d are the amplitude and frequency of the drive field (DF) along the z-direction, respectively. In addition, $R_{s,i}$ (T/s) is the slew rate (SR) of the FF, G_i is the selection field gradient, and FOV_i is the FOV along direction i . The

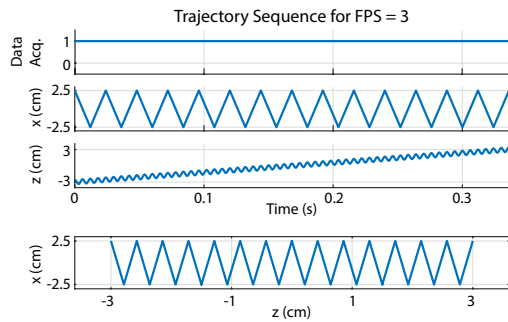


Figure 1: An example 2D trajectory for the case of FPS = 3. The trajectory covers a $5 \times 6 \text{ cm}^2$ FOV. A triangle-wave motion along the x-direction, a linear motion along the z-direction, and a DF along the z-direction are utilized.

total scan time per frame is equal to $T_s = \text{FOV}_z G_z / R_{s,z}$. The frame rate is then $\text{FPS} = T_s^{-1}$.

Due to time-varying FFs, the FFP movement is not symmetrical around the partial field-of-view (pFOV) centers. This movement causes an additional distortion in the mirror symmetry of the signal, even for the adiabatic case of $\tau = 0$. Assuming that the FFP speed is dominated by the DF, the FF-induced distortion can be modeled as a time shift and an amplitude scaling between the two half cycles of a signal [7]. After distortion correction, we compute τ for each pFOV using TAURUS, by recovering the underlying mirror symmetry between the two half cycles of a DF period of the signal [6].

II.II. Simulations

The simulations were carried out using a custom toolbox in MATLAB (Mathworks, Natick, MA), using the following parameters: $(G_x, G_y, G_z) = (-4.8, 2.4, 2.4) \text{ T/m}$, $f_d = 20 \text{ kHz}$, and $B_p = 10 \text{ mT}$. The MNP responses were generated at 50 MS/s , and then downsampled to 2 MS/s . The signal-to-noise ratio (SNR) was set to 20. A zero-phase finite impulse response band-pass filter with the low and high cut-off frequencies of $1.5f_d$ and $10.5f_d$ was utilized for simultaneous direct feed-through filtering and high frequency noise removal.

In Fig. 2.(a), the $5 \times 6 \text{ cm}^2$ vasculature phantom used in the simulations is shown. The vessel structure had $\geq 2.5 \text{ mm}$ diameter around the main branch and the catheter had 0.83 mm diameter. The relaxation effects were incorporated using the phenomenological model in [8]. The vessel structure contained MNPs with $\tau = 4 \mu\text{s}$ and the catheter was labeled with MNPs that had $\tau = 2 \mu\text{s}$. Single-core monodisperse MNPs with 25 nm core diameter were assumed.

Two different simulations were performed. In the first simulation, the performances at three different FPS levels were compared for a $5 \times 6 \text{ cm}^2$ FOV. FPS levels of 3, 4.2, and 7 were achieved by setting $R_{s,z}$ to 0.43, 0.6, and

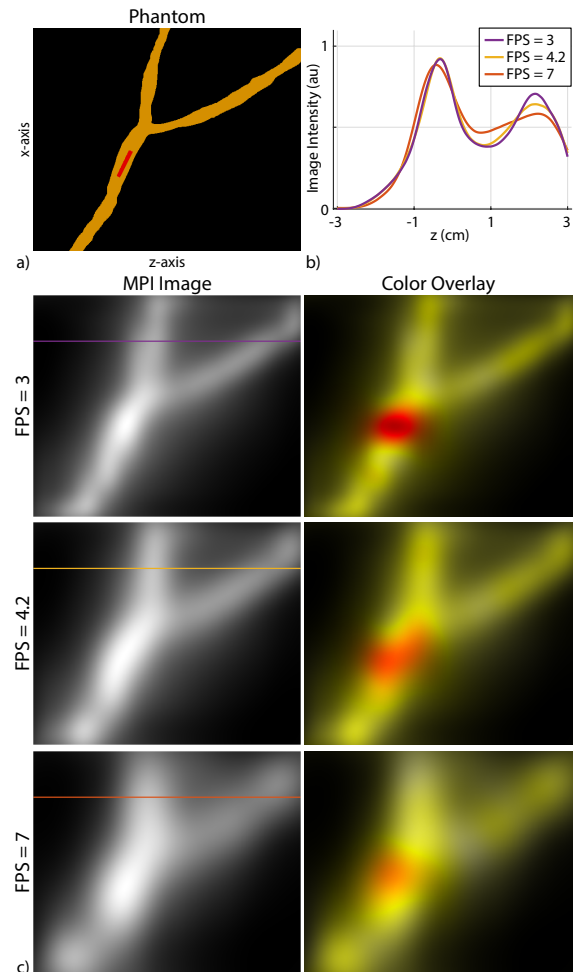


Figure 2: Color MPI simulation results. (a) The vasculature phantom containing a labeled catheter. (b) 1D cross-sections of MPI images at different FPS levels. (c) MPI images and color overlays for FPS = 3, 4.2, and 7. The colored lines mark the 1D cross-sections shown in (b). The labeled catheter can be easily distinguished in the color overlay images at all FPS levels.

1 T/s , respectively. In the second simulation, a reduced FOV of $2.5 \times 3 \text{ cm}^2$ was scanned to zoom into a smaller ROI. A higher FPS level of 9.25 was achieved by setting $R_{s,z}$ to 0.7 T/s . In all of the simulations, $R_{s,x}$ was 20 T/s .

II.III. Image Reconstruction

Image reconstruction consisted of three steps: First, Harmonic Dispersion X-space (HD-X) reconstruction was utilized to reconstruct the MPI images [9]. Because the data points from the 2D triangle trajectory were on a non-Cartesian grid, an automated gridding algorithm for non-Cartesian x-space reconstruction was adapted on the HD-X data [10]. Next, FF-induced time-shift and amplitude scaling distortions were corrected [7]. TAURUS was then applied for each DF period and the estimated τ value was placed on the corresponding pFOV center

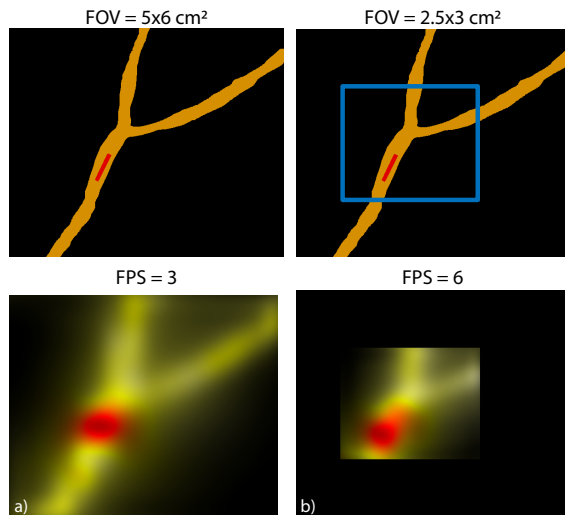


Figure 3: Color MPI simulation results at a higher FPS level for a zoomed-in ROI. Color overlay images are shown for (a) $5 \times 6 \text{ cm}^2$ FOV imaged at FPS = 3 and (b) a reduced FOV of $2.5 \times 3 \text{ cm}^2$ imaged at FPS = 9.25.

location to form a non-Cartesian τ map. The aforementioned gridding algorithm was utilized to reconstruct the Cartesian τ map. Finally, the color MPI image was generated by overlaying the τ map with the MPI image.

III. Results and Discussion

Figure 2 shows the results for the FPS levels of 3, 4.2, and 7. The labeled catheter can be easily distinguished in the color overlay images at all FPS levels tested. In Fig. 2.(c), rapid TAURUS estimates τ within the vasculature structure as $4 \mu\text{s}$. On the other hand, τ for the labeled catheter is estimated as $3.4 \mu\text{s}$, which is higher than the original $2 \mu\text{s}$. This result is expected, since TAURUS estimates a weighted average τ in regions that contain a mixture of MNPs with different τ values, as explained in [6].

As seen in Fig. 2, the fidelity of both the MPI image and the color overlay decreases with FPS. This result is a direct consequence of the reduced trajectory density at higher FPS levels. Note that the trajectory density is a function of the SRs due to Eq. (1). Increasing the FPS requires $R_{s,z}$ to be increased. To maintain trajectory density and image resolution, $R_{s,x}$ would have to be increased at the same rate as $R_{s,z}$. In this work, $R_{s,x}$ was fixed to 20 T/s considering potential hardware and safety limitations. With $R_{s,x}$ fixed, higher FPS levels resulted in reduced trajectory density, and thereby reduced image resolution.

Figure 3 shows that higher FPS levels can be achieved by zooming into a smaller ROI (chosen manually in this case). In Fig. 3.(a), first, the $5 \times 6 \text{ cm}^2$ FOV was scanned at 3 FPS to locate the catheter tip. In Fig. 3.(b), a reduced FOV of $2.5 \times 3 \text{ cm}^2$ was scanned at 9.25 FPS, resulting in a slightly higher resolution image with more than 3 times

the FPS.

For the real-time application, image reconstruction should be faster than T_s . For a single DF period, the average execution time of rapid TAURUS followed by τ map gridding was 0.75 ms, and that of HD-X followed by gridding was 0.6 ms, on an Intel i5-10600k with Windows 10. Considering that $f_d = 20 \text{ kHz}$, the execution time per period corresponds to approximately 15 periods. Rapid TAURUS, HD-X, and gridding only require the individual DF periods and can be parallelized to run on different processor cores or a GPU for each DF period. Additionally, τ map generation and image reconstruction are completely separate processes. Therefore, an efficient implementation in a different programming language and parallelization can enable real-time reconstruction.

IV. Conclusion

In this work, we presented the first simulation results demonstrating the feasibility of real-time color MPI using rapid TAURUS. The results show that color MPI images can be successfully generated for a relatively wide FOV at frame rates exceeding 5 FPS. Additionally, a smaller ROI can be scanned at frame rates exceeding 9 FPS, without sacrificing from image fidelity.

Acknowledgments

This work was supported by the Scientific and Technological Research Council of Turkey (Grant No: TUBITAK 120E208).

Author's statement

Conflict of interest: Authors state no conflict of interest.

References

- [1] J. Rahmer, D. Wirtz, C. Bontus, J. Borgert, and B. Gleich. Interactive magnetic catheter steering with 3-d real-time feedback using multi-color magnetic particle imaging. *IEEE Trans. Med. Imag.*, 36(7):1449–1456, 2017, doi:10.1109/TMI.2017.2679099.
- [2] Y. Shi and J. B. Weaver. Concurrent quantification of magnetic nanoparticles temperature and relaxation time. *Medical physics*, 46(9):4070–4076, 2019, doi:10.1002/mp.13655.
- [3] S. Draack, M. Schilling, and T. Viereck. Magnetic particle imaging of particle dynamics in complex matrix systems. *Physical Sciences Reviews*, 2021, doi:doi:10.1515/psr-2019-0123.
- [4] M. Utkur, Y. Muslu, and E. U. Saritas. Relaxation-based color magnetic particle imaging for viscosity mapping. *Applied Physics Letters*, 115(15):152403, 2019, doi:10.1063/1.5110475.
- [5] P. Szwargulski, M. Wilmes, E. Javidi, F. Thieben, M. Graeser, M. Koch, C. Gruettner, G. Adam, C. Gerloff, T. Magnus, *et al.* Monitoring intracranial cerebral hemorrhage using multicontrast real-time magnetic particle imaging. *ACS nano*, 14(10):13913–13923, 2020, doi:10.1021/acsnano.0c06326.

- [6] Y. Muslu, M. Utkur, O. B. Demirel, and E. U. Saritas. Calibration-free relaxation-based multi-color magnetic particle imaging. *IEEE Trans. Med. Imag.*, 37(8):1920–1931, 2018, doi:[10.1109/TMI.2018.2818261](https://doi.org/10.1109/TMI.2018.2818261).
- [7] M. T. Arslan, A. A. Özaslan, S. Kurt, Y. Muslu, and E. U. Saritas, Rapid taurus for relaxation-based color magnetic particle imaging, 2021. arXiv: [2112.04880](https://arxiv.org/abs/2112.04880) [eess.SP].
- [8] L. R. Croft, P. W. Goodwill, and S. M. Conolly. Relaxation in x-space magnetic particle imaging. *IEEE Trans. Med. Imag.*, 31(12):2335–2342, 2012, doi:[10.1109/TMI.2012.2217979](https://doi.org/10.1109/TMI.2012.2217979).
- [9] S. Kurt, V. Abdulla, and E. U. Saritas. Multi-dimensional harmonic dispersion x-space mpi. *Int. J. Magn. Part. Imaging*, 6(2 Suppl 1), 2020, doi:[10.18416/IJMPI.2020.2009062](https://doi.org/10.18416/IJMPI.2020.2009062).
- [10] A. Ozaslan, A. Alacaoglu, O. Demirel, T. Çukur, and E. Saritas. Fully automated gridding reconstruction for non-cartesian x-space magnetic particle imaging. *Physics in Medicine & Biology*, 64(16):165018, 2019, doi:[10.1088/1361-6560/ab3525](https://doi.org/10.1088/1361-6560/ab3525).